**Supporting Information**

# Metal Halide Perovskite and Perovskite–like Materials Through the Lens of Ultra–wideline $^{35/37}$Cl NMR Spectroscopy

Diganta Sarkar,[a] Riley W. Hooper,[a] Abhoy Karmakar,[a] Amit Bhattacharya,[a] Arkadii Pominov,[a] Victor V. Terskikh,[b] and Vladimir K. Michaelis*,[a]

[a]*Department of Chemistry, University of Alberta, Edmonton, Alberta T6G 2G2, Canada*

[b] *Metrology, National Research Council of Canada, Ottawa, Ontario K1A 0R6, Canada*

**Corresponding author: vladimir.michaelis@ualberta.ca*

# Table of Contents

# Materials and Methods

## Experimental

All starting materials were purchased from commercial sources and used without further purification: Cesium chloride (CsCl, 99%), and methylamine hydrochloride (MACl, 98%) from Sigma Aldrich (St. Louis, MO, USA); formamidine hydrochloride (FACl, 97%) from Sigma Aldrich (Oakville, ON, Canada); lead(II) chloride ($PbCl_2$, 99%) from ACROS Organics (Morris Plains, NJ, USA).

## Synthesis

### a. Ball–milling Synthesis of $FAPbCl_3$

Due to the excessive hygroscopic nature of FACl, an argon–filled glove box was used for mixing of FACl (1 mmol, 81 mg) and $PbCl_2$ (1 mmol, 278 mg) in 1 : 1 molar ratio, and ground in an agate mortar for 2–3 minutes. The mixture was transferred to a 50–mL vacuum/inert gas stainless–steel lined zirconia grinding jar equipped with ~90 g of zirconia balls (with diameters of 3, 5, and 8 mm) and sealed within the glove box. The sample was removed from the glove box and ball–milled for 60 minutes at 750 rpm using an electric planetary ball mill instrument (Changsha Deco–PBM–V–0.4L) under ambient laboratory conditions. The grinding jar was then opened inside a glove box, and the sample was removed by scraping the inner wall of the jar using a clean spatula. The procedure was repeated two times for a total grinding time of 120 minutes to obtain the $FAPbCl_3$.

### b. Ball–milling Synthesis of $FA_{0.50}MA_{0.50}PbCl_3$

MACl (0.5 mmol, 34 mg), FACl (0.5 mmol, 41 mg) and $PbCl_2$ (1 mmol, 278 mg) in 1 : 1 : 2 molar ratios, and ground in an agate mortar for 2–3 minutes inside an argon–filled glove box. Then similar procedures for the ball–milling synthesis of $FAPbCl_3$ (above) were followed with a total grinding time of 60 minutes to obtain the final product, $FA_{0.50}MA_{0.50}PbCl_3$.

### c. Ball–milling Synthesis of $MAPbCl_3$

MACl (1.5 mmol, 101 mg) and $PbCl_2$ (1.5 mmol, 417 mg) were mixed in 1 : 1 molar ratio, and ground together in an agate mortar for 2–3 minutes. The mixture was transferred to a 50–mL zirconia grinding jar equipped with ~50 g of zirconia balls (diameters of 3, 5, and 8 mm) and sealed. An electric planetary ball mill instrument (Changsha Deco–PBM–V–0.4L) was used for ball–milling of the mixture for 15 minutes at 750 rpm under ambient laboratory conditions, and a clean spatula was used to scrape the inner wall of the jar. The procedure was repeated four times for a total grinding time of 60 minutes to obtain the $MAPbCl_3$.

### d. Ball–milling Synthesis of $CsPb(Cl_{0.03}Br_{0.97})_3$

CsBr (~1.9 mmol, 404 mg), CsCl (~0.3 mmol, 51 mg), and $PbBr_2$ (~1.9 mmol, 697 mg) were added to a 12 mL stainless steel grinding jar filled with approx. 30 stainless steel balls (5 mm diameter). The reagents were ball–milled in a Retsch PM–100 planetary mill for 3x30 minute intervals (total grinding time 1.5 hr) at 500 rpm, using a spatula to scrape the inner walls of the jar between

grinding times to ensure intimate mixing of reagents. Milled sample was then annealed at 150°C for 1 hr before characterization.

### e. Synthesis of Remaining Perovskite and Perovskite–like Compounds

The remaining compounds were synthesized as described previously. The detailed procedure for the mechanochemical synthesis of 3D $CsPb(Cl_xBr_{1-x})_3$ (x = 0.33, 0.67, and 1.0), 2D $CsPb_2Cl_5$ and 0D $Cs_4PbCl_6$ can be found in ref[1]. The inverse temperature crystallization (ITC) synthesis of $MAPbCl_3$ and mechanochemical synthesis of $MAPb(Cl_xBr_{1-x})_3$ (x = 0.25, 0.50, and 0.75) are discussed in ref[2]. The $Cs_2B'AgCl_6$ (B' = Bi and In) were prepared via solvent synthesis (SS) and the details are discussed in ref[3]. The solvent synthesis procedure of $CsGeCl_3$ can be found in ref[4].

## Powder X–ray Diffraction (XRD)

The powder XRD measurements were performed under ambient laboratory conditions on a Bruker D8 AVANCE diffractometer (40 kV, 20 mA) system (Department of Chemistry, University of Alberta) equipped with an SSD160 detector and Cu Kα radiation source (Cu–$K_{\alpha1}$ (λ = 1.5406 Å) and $K_{\alpha2}$ (λ = 1.5444 Å) radiation). A zero diffraction Si crystal plate (24.6 mm diameter x 1.0 mm thickness) was used for placing the samples and obtaining the 2θ scans between 5° to 90° with a step increment of 0. 0197°. FullProf suite of software[5] was used for profile fitting and refinement of the unit cell parameters of $FA_{0.50}MA_{0.50}PbCl_3$ and $CsPb(Cl_xBr_{1-x})_3$ (x = 0.03, 0.33, and 0.67) compounds.

## Energy–dispersive X–ray (EDX) Spectroscopy and Scanning Electron Microscopy (SEM)

To determine the chemical composition of $CsPb(Cl_{0.03}Br_{0.97})_3$, EDX spectroscopy was performed using a Zeiss Sigma 300 VP Field Emission Scanning Electron Microscope (accelerating voltage of 5–20 kV) equipped with secondary and backscattered electron detectors, an in–lens detector, and an energy dispersive X–ray (EDX) spectrometer. Samples were prepared by applying powders onto carbon tape using an aluminium stub.

## Solid–state $^{35}$Cl Nuclear Magnetic Resonance (NMR) Spectroscopy

### a. 7.05 T NMR Data

NMR data at 7.05 T were acquired at room temperature under non–spinning conditions using 4 mm $ZrO_2$ rotors (150–200 mg of sample) on a Bruker AVANCE NEO 300 NMR spectrometer. The frequency–stepped wide–band, uniform, and smooth truncation Carr–Purcell–Meiboom–Gill (WURST–CPMG)[6,7] pulse sequence was used to record the $^{35}$Cl NMR spectra for each compound using a 4 mm double resonance H/X Bruker probe. The variable offset cumulative spectrum (VOCS) technique[8] was used to acquire the $^{35}$Cl NMR sub–spectra with different frequency offsets; these spectra were added to obtain the complete full spectrum. For $CsPb(Cl_xBr_{1-x})_3$ (x = 0.03, 0.33, and 0.67), the wideline spectra were obtained by displaying the skyline projection of a series of sub–spectra. Each sub–spectrum was acquired using the following common experimental parameters: number of echoes = 50, spikelet spacing = 5 kHz, and WURST excitation spectral width = 1 MHz. Other parameters used for all the samples are summarized in Table S1.

**Table S1.** Non−spinning $^{35}$Cl NMR experimental parameters used in VOCS employing the WURST−CPMG pulse sequence at 7.05 T. All the samples were mechanochemically synthesized unless mentioned.

| Samples | Recycle Delays (s) | # of Scans | # of Sub−spectra | Frequency Step (kHz) | Total Acquisition Time (Hours) |
|---|---|---|---|---|---|
| $Cs_2InAgCl_6$ (SS) | 1.0 | 1,536 | 15 | 250 | 6.6 |
| $Cs_2InAgCl_6$ (SS) | 1.0 | 3,072 | 11 | 250 | 9.8 |
| $CsGeCl_3$ (SS) | 0.2 | 8,000 | 8 | 350 | 4.5 |
| $FAPbCl_3$ | 0.2 | 5,120 | 6 | 250 | 2.0 |
| $FA_{0.50}MA_{0.50}PbCl_3$ | 0.2 | 5,120 | 6 | 250 | 2.0 |
| $MAPbCl_3$ | 0.2 | 5,120 | 6 | 250 | 2.0 |
| $MAPbCl_3$ (ITC synthesized) | 0.1 | 10,000 | 5 | 250 | 1.9 |
| [a]$MAPb(Cl_xBr_{1-x})_3$ (x = 0.25, 0.50, 0.75) | 0.2 | 45,000 | 3 | 500 | 9.0 |
| $CsPbCl_3$ | 0.5 | 10,000 | 5 | 250 | 7.5 |
| $CsPb(Cl_{0.03}Br_{0.97})_3$ | 0.2 | 100,000 | 5 | 250 | 33.3 |
| $CsPb(Cl_{0.33}Br_{0.67})_3$ | 0.2 | 153,600 | 3 | 500 | 30.8 |
| $CsPb(Cl_{0.67}Br_{0.33})_3$ | 0.2 | 153,600 | 3 | 500 | 30.8 |
| $CsPb_2Cl_5$ | 1.5 | 10,000 | 6 | 250 | 25.6 |
| $Cs_4PbCl_6$ | 0.2 | 10,000 | 2 | 250 | 1.3 |

[a]Spectra were not shown due to limitations in S/N.

Additionally, a non−spinning $^{35}$Cl NMR spectrum of ITC−synthesized $MAPbCl_3$ was also acquired at room temperature using the same probe by employing a Hahn−echo pulse sequence.[9] A recycle delay of 0.1 s was used, with 13 VOCS steps and a frequency step size of 100 kHz were used to obtain a final spectrum after adding all the sub−spectra. All the $^{35}$Cl NMR spectra at 7.05 T were referenced to a secondary standard (solid CsCl, $\delta(^{35}Cl)$ = 114 ppm) with respect to primary standard of 1 M NaCl in $H_2O$ ($\delta(^{35}Cl)$ = 0.00 ppm).

## b. 21.1 T NMR Data

Non−spinning $^{35}$Cl NMR spectra at 21.1 T were acquired on a Bruker Avance II 900 NMR spectrometer using a home−built 4 mm H/X low−E solenoid probe at room temperature. Samples were packed in 4 mm $ZrO_2$ Bruker rotors, thin−walled (~150 mg) or thick walled (~75 mg) depending on the sample volume. WURST−CPMG, WURST−echo,[7] and quadrupolar−echo[10,11] pulse sequences were used for all the samples with a primary reference of 1 M KCl in $D_2O$ at $\delta(^{35}Cl)$ = 0.00 ppm; the experimental parameters for the experiments are discussed below.

**WURST−CPMG** NMR spectra of the mechanochemically synthesized samples were acquired using a WURST excitation spectral width of 2 MHz, 48 echoes, a spikelet spacing of 2 kHz and with proton decoupling when required. Unlike the $^{35}$Cl NMR spectra at 7.05 T, the WURST−CPMG NMR spectra at 21.1 T are obtained in a single step significantly reducing the acquisition time. **WURST−echo** NMR spectra were obtained using the same WURST pulse parameters discussed above, followed by a single echo acquisition. All other relevant WURST−CPMG and WURST−echo experimental parameters for each of the samples are mentioned in Table S2.

**Table S2.** Non–spinning $^{35}$Cl NMR experimental parameters used in WURST–CPMG and WURST–echo pulse sequences at 21.1 T for the mechanochemically synthesized samples.

| Samples | Recycle Delays (s) | # of Scans | | Total Acquisition Time (Hours) | |
|---|---|---|---|---|---|
| | | WURST–CPMG | WURST–echo | WURST–CPMG | WURST–echo |
| [a]$FAPbCl_3$ | 2 | 1,024 | 4,096 | 0.5 | 2.5 |
| [a]$MAPbCl_3$ | 2 | 1,024 | 4,096 | 0.5 | 2.5 |
| $CsPbCl_3$ | 1 | 4,096 | 16,384 | 1.0 | 4.5 |
| $CsPb_2Cl_5$ | 2 | 1,024 | 3,072 | 0.5 | 1.5 |
| $Cs_4PbCl_6$ | 2 | 1,024 | 3,072 | 0.5 | 1.5 |

[a]Proton decoupling was used during WURST–CPMG experiment for these samples.

**Quadrupolar–echo** NMR spectra were obtained by adding different frequency–stepped sub–spectra acquired by employing the VOCS technique with a step size of 150 kHz when required. A recycle delay of 1 s and 16,384 scans were used to record the sub–spectra with acquisition time of = 4.5 hrs per step for all the mechanochemically synthesized samples. Quadrupolar–echo NMR spectra of $FAPbCl_3$ was acquired using five steps with total experimentation time of 22.5 hrs. Similarly, 13.5 hrs were required to obtain the spectra of $MAPbCl_3$, $CsPbCl_3$, and $CsPb_2Cl_5$. The spectrum for $Cs_4PbCl_6$ was recorded in a single step with an acquisition time of 4.5 hrs.

## Solid–state $^{37}$Cl NMR Spectroscopy

A non–spinning $^{37}$Cl quadrupolar–echo NMR spectrum of $CsPbCl_3$ was also acquired at 21.1 T on a Bruker Avance II 900 NMR spectrometer using a home–built 4 mm H/X low–E solenoid probe at room temperature. Approx. 50 mg of $CsPbCl_3$ was packed in a thick–walled 4 mm $ZrO_2$ Bruker rotor. Three sub–spectra were acquired with frequency stepping of 125 kHz to obtain the complete quadrupolar–echo spectrum using a recycle delay of 1 s, 65,536 co–added transients, and a total acquisition time of 18 hrs.

## NMR Data Processing and Analysis

NMR spectra were processed using the Topspin 4.1.1 Bruker software and plotted using the OriginPro 8.5 software. All the $^{35/37}$Cl NMR spectra were fit using the WSolids1 NMR simulation package.[12] Euler angles of the samples were extracted using EFGShield (Version 4.6) to aid in simulation.[13] EFG ellipsoids were visualized using MagresView V 1.6.2.[14]

## Quantum Chemical Computations

The CAmbridge Serial Total Energy Package (CASTEP) software package[15,16] with NMR modules[17,18] were used to perform quantum chemical calculations to compute theoretical NMR interaction parameters. The projector-augmented wave method (PAW) and GGA/PBE functional[19] were used for electronic structure calculations. The complementary GIPAW method was utilized to calculate the NMR parameters. For k-space sampling, k-points were distributed according to Monkhorst-Pack (MP) scheme[20], with grid dimensions of p x q x r and no grid shifting.

The plane wave cut-off energy was set automatically according to elemental composition, with "Extreme" precision setting in CASTEP. The exact cut-off values are given in Table S3.

**Table S3.** MP grid *k*–points and plane wave cut–off energy used for GIPAW–DFT calculations for all the samples.

| Samples | MP grid (p × q × r) *k*–points | Plane Wave Cut–off Energy (eV) |
|---|---|---|
| $Cs_2SnCl_6$ | 8 × 8 × 8 | 392 |
| $Cs_2InAgCl_6$ | 8 × 8 × 8 | 827 |
| $Cs_2BiAgCl_6$ | 8 × 8 × 8 | 827 |
| $CsGeCl_3$ | 12 × 12 × 12 | 567 |
| $FAPbCl_3$ | 12 × 12 × 12 | 750 |
| $MAPbCl_3$ | 12 × 12 × 12 | 750 |
| $CsPbCl_3$ | 10 × 7 × 10 | 750 |
| $CsPb_2Cl_5$ | 8 × 8 × 4 | 750 |
| $Cs_4PbCl_6$ | 5 × 5 × 4 | 392 |
| CsCl (ref.) | 10 × 10 × 10 | 750 |

**Table S4.** Crystal system, space group and cell parameters of the samples used for GIPAW–DFT calculations.

| Samples | Crystal System & Space Group | Cell Parameters | | | | | | Ref. |
|---|---|---|---|---|---|---|---|---|
| | | a (A°) | b (A°) | c (A°) | α (deg.) | β (deg.) | γ (deg.) | |
| $Cs_2SnCl_6$ | Cubic ($Fm\bar{3}m$) | 10.67 | 10.67 | 10.67 | 90 | 90 | 90 | [23] |
| $Cs_2InAgCl_6$ | Cubic ($Fm\bar{3}m$) | 10.48 | 10.48 | 10.48 | 90 | 90 | 90 | [24] |
| $Cs_2BiAgCl_6$ | Cubic ($Fm\bar{3}m$) | 10.78 | 10.78 | 10.78 | 90 | 90 | 90 | [25] |
| $CsGeCl_3$ | Rhombohedral ($R3m$) | 5.45 | 5.45 | 5.45 | 89.72 | 89.72 | 89.72 | [26] |
| $FAPCl_3$ | Cubic ($Pm\bar{3}m$) | 5.74 | 5.74 | 5.74 | 90 | 90 | 90 | [27] |
| $MAPbCl_3$ | Cubic ($Pm\bar{3}m$) | 5.69 | 5.69 | 5.69 | 90 | 90 | 90 | [28] |
| $CsPbCl_3$ | Orthorhombic ($Pnma$) | 7.90 | 11.25 | 7.89 | 90 | 90 | 90 | [29] |
| $CsPb_2Cl_5$ | Tetragonal ($I4/mcm$) | 8.13 | 8.13 | 14.77 | 90 | 90 | 90 | [30] |
| $Cs_4PbCl_6$ | Rhombohedral ($R\bar{3}c$) | 13.18 | 13.18 | 16.64 | 90 | 90 | 120 | [31] |
| CsCl (ref.) | Cubic ($Pm\bar{3}m$) | 4.11 | 4.11 | 4.11 | 90 | 90 | 90 | [32] |

All unit–cell parameters and atomic coordinates were taken from their corresponding crystal structures as summarised in Table S4. Hydrogen atoms were inserted in the MA and FA cations for hybrid MA– and $FAPbCl_3$ unit cells using the Avogadro software,[21,22] and geometry optimization of the H positions were performed before calculating NMR parameters. The *k*–point

grid dimension parameters (p × q × r) were increased until the computed values of the magnetic shielding tensor converged to $\Delta\sigma_{computed} \leq 1$ ppm. Finally, GIPAW–DFT computed $^{35}$Cl magnetic shielding tensor values were converted to chemical shifts using the computed values of CsCl as a reference sample with $\delta$(ppm) ≈ $\sigma_{ref}$ (ppm) – $\sigma_{computed}$ (ppm), where $\sigma_{ref}$ = 914.75 ppm was used to match the $\delta_{iso}$ = 114 ppm value obtained from the experimental $^{35}$Cl solid CsCl spectrum at 7.05 T.

## NMR Parameter Definitions

Detailed discussion about several solid–state NMR interactions and parameters can be found elsewhere.[33,34] Relevant NMR parameters mentioned in this study are briefly discussed below:

### a. Isotropic chemical shift ($\delta_{iso}$)

$\delta_{iso}$ is the result of averaging the principal components of the anisotropic shift tensor. Chemical shift values ($\delta$) are obtained by converting the magnetic shielding values ($\sigma$) in reference to a standard with a specified chemical shift.

In the principal axis frame, the magnetic shielding tensor can be represented as:

$$\sigma = \begin{pmatrix} \sigma_{11} & 0 & 0 \\ 0 & \sigma_{22} & 0 \\ 0 & 0 & \sigma_{33} \end{pmatrix}$$

The diagonal components of the magnetic shielding tensor can be converted to chemical shift values using the following relation:

$$\delta_{ii} = \frac{\sigma_{ref} - \sigma_{ii}}{1 - \sigma_{ref}} \approx (\sigma_{ref} - \sigma_{ii}), i = 1, 2, 3$$

where, the magnetic shielding of $^{35/37}$Cl reference, $\sigma_{ref}$ is considered to be $\ll 1$ to obtain the simplified equation for chemical shift values ($\delta_{ii}$), and the isotropic chemical shift is given by the following equation:

$$\delta_{iso} = \frac{\delta_{11} + \delta_{22} + \delta_{33}}{3}$$

### b. Quadrupole coupling constant ($C_Q$)

Nuclei with nuclear spin, $I > 1/2$ are quadrupolar and have a nuclear quadrupolar moment ($Q_m$). This $Q_m$ couples with the electric field gradient (EFG) generated by the electric field produced by the electronic charge distribution of its surrounding chemical environment, giving rise to the quadrupolar interaction (QI). The strength of the QI can be understood by the quadrupole coupling constant ($C_Q$) value, which has a direct relation to the largest principal component of the EFG tensor at the nucleus ($V_{ZZ}$) and $Q_m$, and is defined by the equation:

$$C_Q = \frac{eQ_mV_{ZZ}}{h}$$

where $e$ = charge of the electron, and $h$ = Planck's constant.

### c. Asymmetry parameter ($\eta$)

The deviation of the EFG from axial symmetry can be obtained from the asymmetry parameter, $\eta$, given by the equation:

$$\eta = \frac{V_{XX} - V_{YY}}{V_{ZZ}}, (0 \leq \eta \leq 1)$$

where three principal components of EFG tensor follow the trend $|V_{XX}| \leq |V_{YY}| \leq |V_{ZZ}|$.

# Powder XRD Data

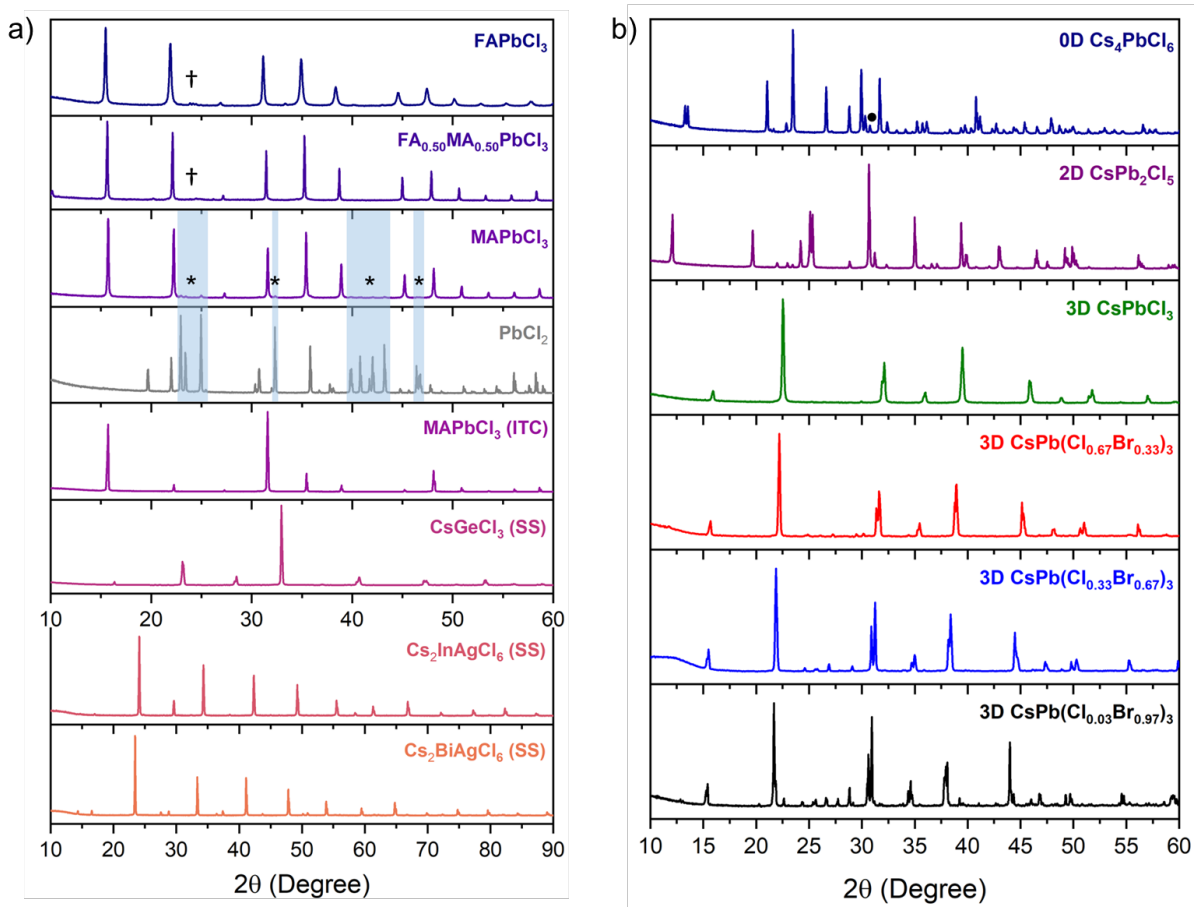


**Figure S1.** Room–temperature powder XRD patterns of those samples whose NMR spectra are shown in this study. (a) hybrid 3D $FAPbCl_3$, $FA_{0.50}MA_{0.50}PbCl_3$, $MAPbCl_3$, $CsGeCl_3$, $Cs_2InAgCl_6$, and $Cs_2BiAgCl_6$. (b) 0D $Cs_4PbCl_6$, 2D $CsPb_2Cl_5$, and 3D $CsPb(Cl_xBr_{1-x})_3$ (x = 1, 0.67, 0.33, and 0.03). All compounds were prepared by mechanochemical synthesis unless mentioned [ITC = inverse temperature crystallization, SS = solvent synthesis]. $FAPbCl_3$ and $FA_{0.50}MA_{0.50}PbCl_3$ has an unidentified impurity, denoted by the daggers (†) in (a). The asterisks (*) indicate the presence of $PbCl_2$ as starting material in mechanochemically synthesized $MAPbCl_3$ in (a). CsCl was assigned as the impurity in $Cs_4PbCl_6$ in a previous study by Karmakar *et al.*[1] and is denoted by black circle (●) in (b).

**Table S5.** Refined unit cell parameters from PXRD patterns.

| **Materials** | | **$FA_{0.50}MA_{0.50}PbCl_3$** | **$CsPb(Cl_xBr_{1-x})_3$** | | |
|---|---|---|---|---|---|
| | | | **x = 0.03** | **x = 0.33** | **x = 0.67** |
| Crystal System | | Cubic | Orthorhombic | Orthorhombic | Orthorhombic |
| Space Group | | $Pm\bar{3}m$ | *Pnma* | *Pnma* | *Pnma* |
| Cell Parameters | a (Å) | 5.7121(4) | 8.2303(15) | 8.2735(18) | 8.2855(13) |
| | b (Å) | 5.7121(4) | 11.7359(17) | 11.4954(17) | 11.3495(21) |
| | c (Å) | 5.7121(4) | 8.1953(16) | 8.1593(12) | 8.0439(20) |
| | Angles | α = β = γ = 90° | α = β = γ = 90° | α = β = γ = 90° | α = β = γ = 90° |
| Volume (V) (Å$^3$) | | 186.37(2) | 791.583(24) | 776.02(24) | 756.41(26) |
| *Z* | | 1 | 4 | 4 | 4 |
| Formula Unit Volume (Å$^3$) | | *V*/*Z* = 186.37 | *V*/*Z* = 197.90 | *V*/*Z* = 194.01 | *V*/*Z* = 189.10 |

# A–site Variation of 3D Perovskites Data

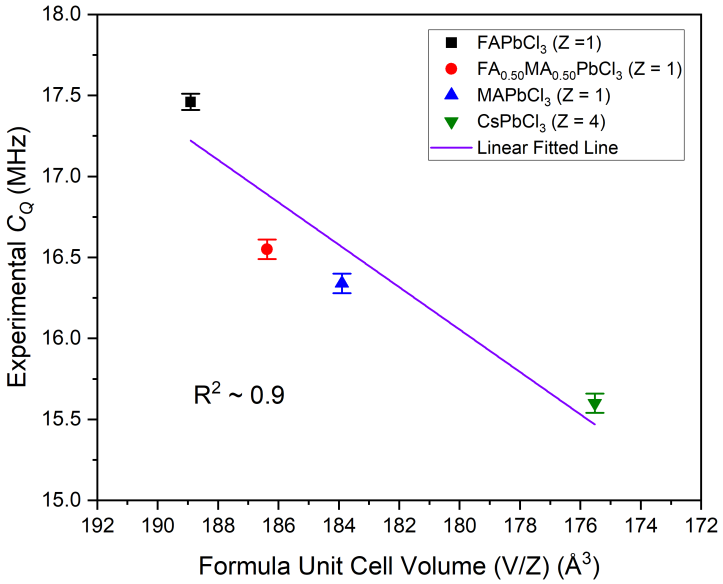


**Figure S2.** DPlot of experimental (WURST–CPMG) $^{35}$Cl $C_Q$ on the formula unit cell volume ($V/Z$) with A–site variation for 3D LHPs.

# Energy–dispersive X–ray (EDX) Spectroscopy Data and Scanning Electron Microscopy (SEM) Images

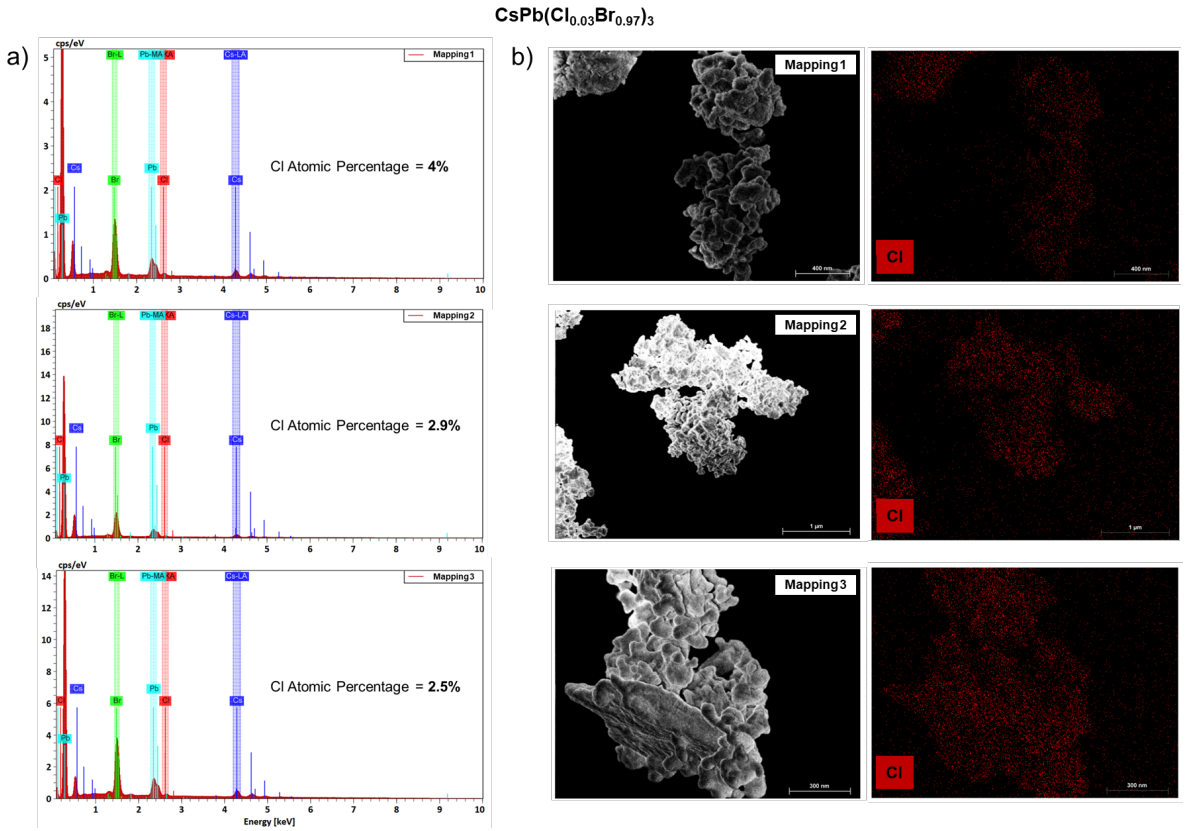


**Figure S3.** (a) Elemental analysis via EDX spectroscopy for $CsPb(Cl_{0.03}Br_{0.97})_3$ (in triplicate as shown from top to bottom). (b) SEM images and the corresponding EDX elemental mapping for Cl of $CsPb(Cl_{0.03}Br_{0.97})_3$. The average from the three elemental mappings provided the atomic % of Cl of ~3% in the sample.

# Solid–state $^{35}$Cl NMR Spectroscopy Data

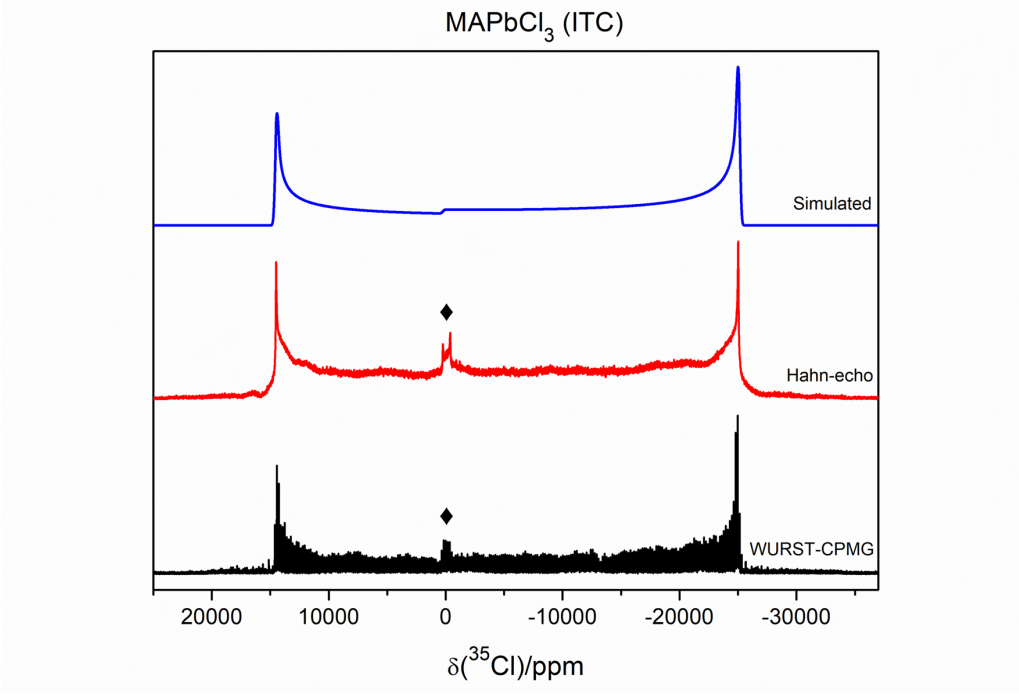


**Figure S4.** Non–spinning $^{35}$Cl WURST–CPMG (black), and Hahn–echo (red) NMR spectra of ITC-synthesized $MAPbCl_3$ acquired at 7.05 T and 293 K. The simulated spectrum is shown at the top (blue) which yielded NMR parameters of $C_Q$ = 16.34 ± 0.05 MHz, $\eta$ = 0.00 ± 0.02, and $\delta_{iso}$ = 150 ± 125 ppm. The signals denoted by the black diamond suit (◆) arise from an unidentified source.

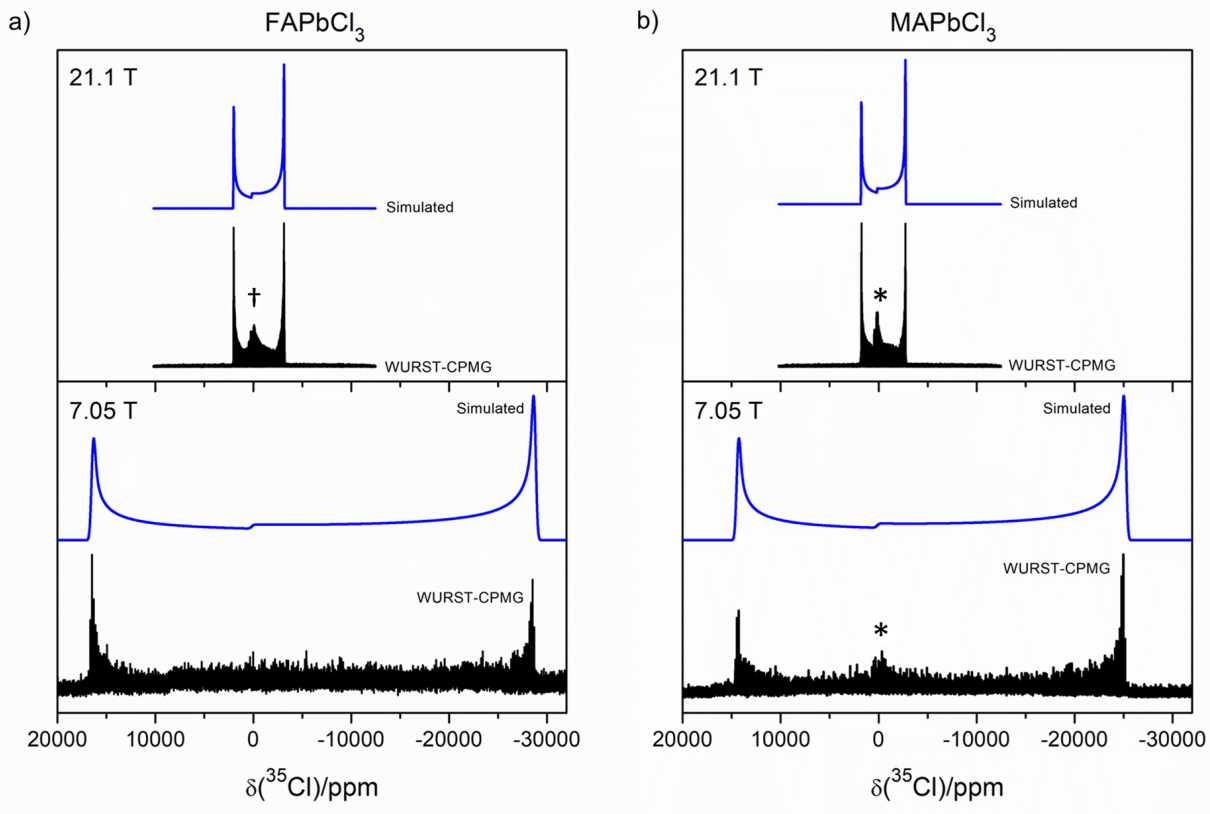

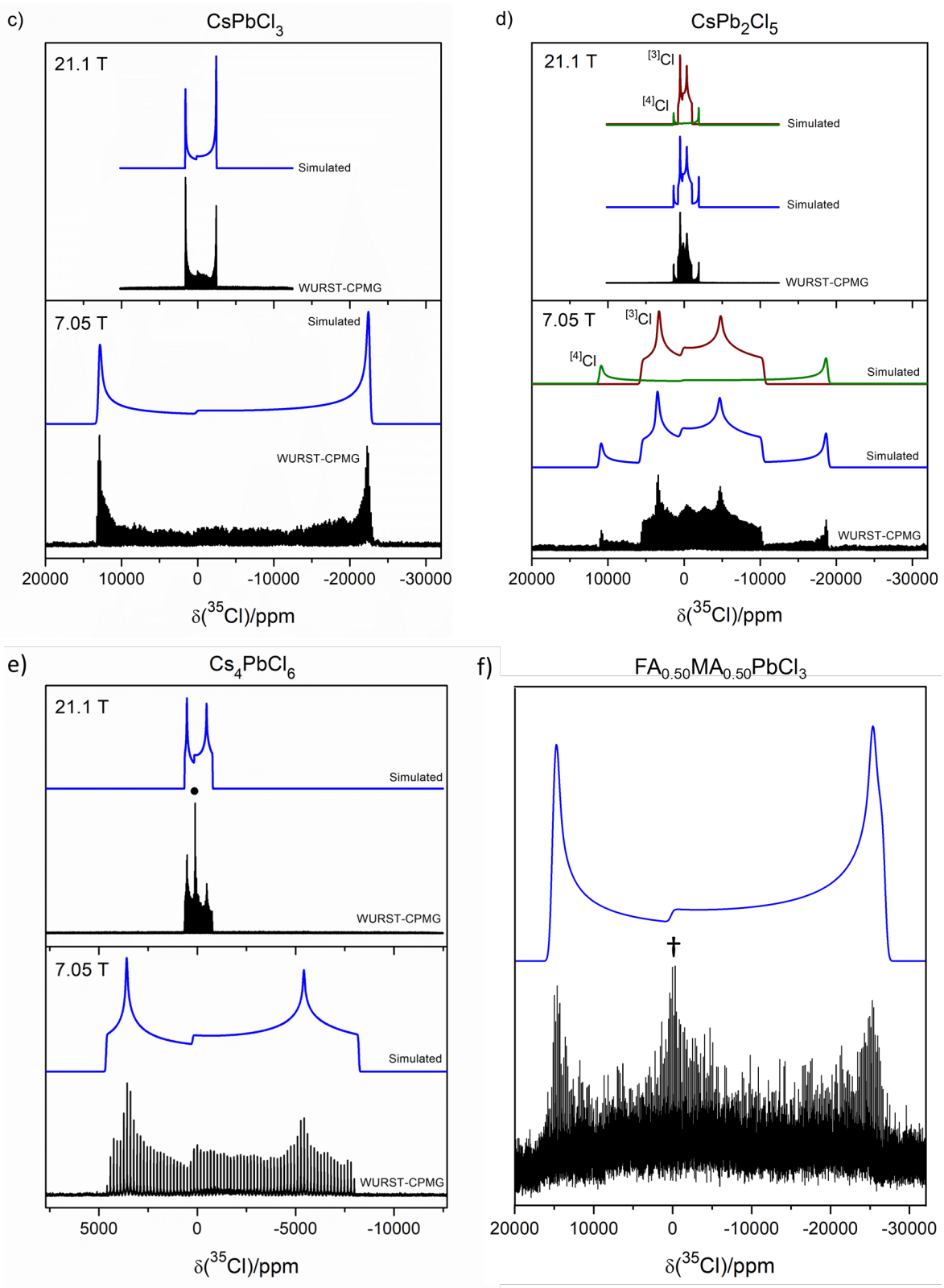


**Figure S5.** Non–spinning $^{35}$Cl WURST–CPMG experimental (black) and simulated (blue) NMR spectra acquired at 21.1 T (top) and 7.05 T (bottom) for (a) $FAPbCl_3$, (b) $MAPbCl_3$, (c) $CsPbCl_3$, (d) $CsPb_2Cl_5$, and (e) $Cs_4PbCl_6$. (f) Non–spinning $^{35}$Cl WURST–CPMG experimental (black) and simulated (blue) NMR spectra of $FA_{0.50}MA_{0.50}PbCl_3$ acquired at 7.05 T. All the samples were mechanochemically synthesized. The individual simulations of two different $^{35}$Cl sites, three–coordinated Cl ($^{[3]}$Cl in brown) and four–coordinated Cl ($^{[4]}$Cl in green) in $CsPb_2Cl_5$ are shown above the simulated spectra in (d) for both magnetic fields. The signals denoted by the daggers (†), asterisks (*), and black circle (●) in (a) and (f), (b), and (e), respectively, correspond to the impurities discussed in the caption to Figure S1.

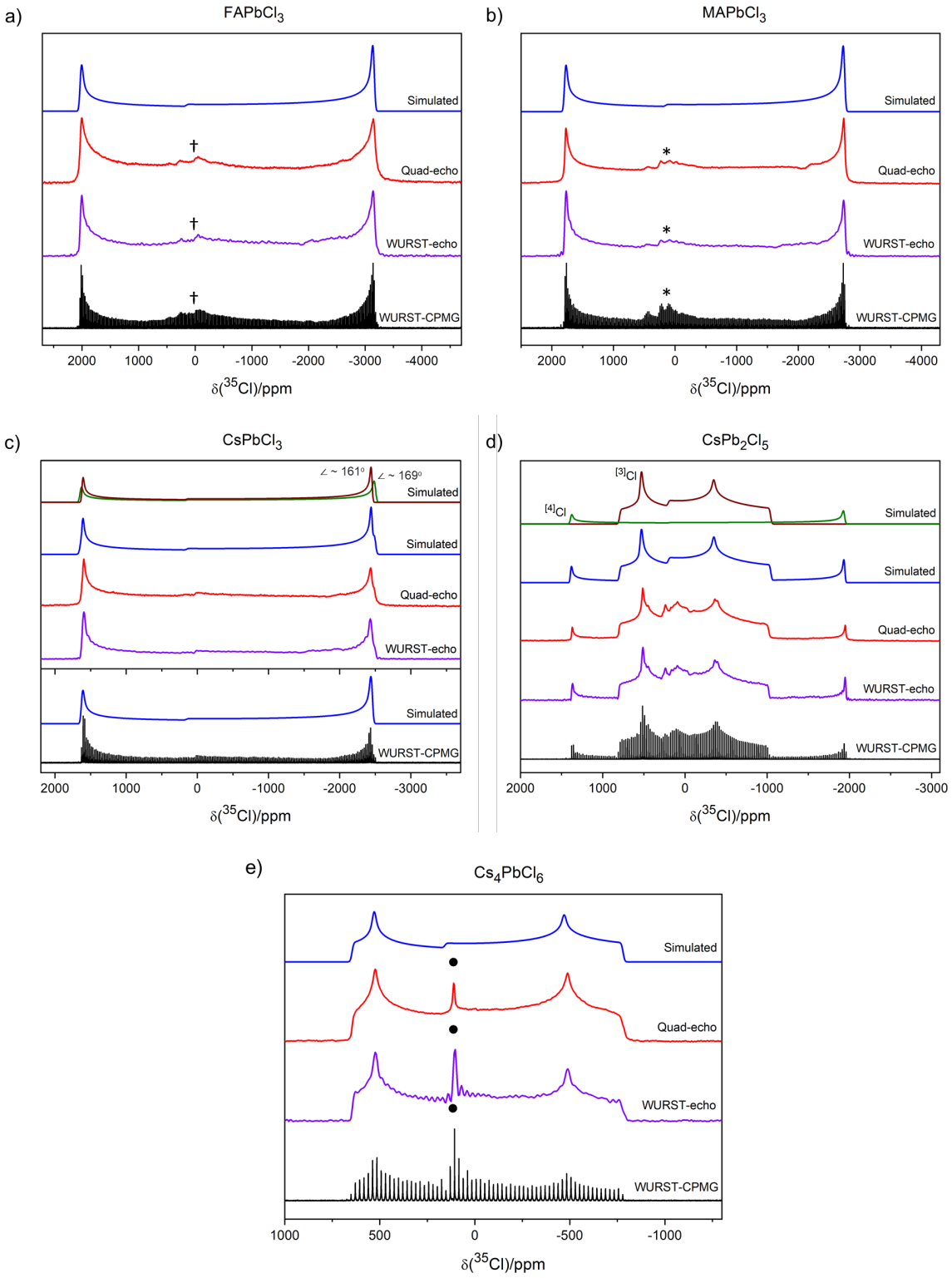


**Figure S6.** Non–spinning $^{35}$Cl WURST–CPMG (black), WURST–echo (violet), quadrupolar–echo (red) NMR spectra and their corresponding simulated (blue) spectra at 21.1 T for mechanochemically synthesized (a) $FAPbCl_3$, (b) $MAPbCl_3$, (c) $CsPbCl_3$, (d) $CsPb_2Cl_5$, and (e) $Cs_4PbCl_6$. Though resolution between two $^{35}$Cl sites with slightly different Pb–Cl–Pb bond angles (∠) in $CsPbCl_3$ was not clear in WURST–CPMG spectrum, it was obtained in WURST–echo and quadrupolar–echo spectra, and individual simulations of the ∠ ~161° (brown) and 169° (green) sites are shown in (c). $CsPb_2Cl_5$ also displayed resolution between two different $^{35}$Cl sites, and three–coordinated Cl ($^{[3]}$Cl in brown) and four–coordinated Cl ($^{[4]}$Cl in green) are shown by individual simulations in (d). The impurities discussed in Figure S1 gave rise to the signals denoted by daggers (†), asterisks (*), and black circles (●) in (a), (b), and (e), respectively.

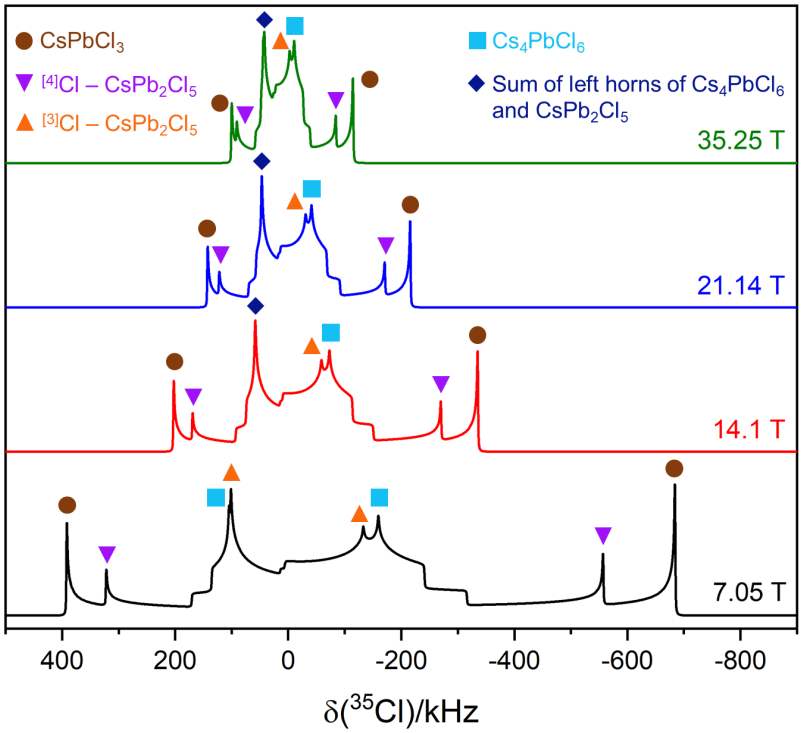


**Figure S7.** Superimposed simulated NMR spectra of 3D $CsPbCl_3$, 2D $CsPb_2Cl_5$ and 0D $Cs_4PbCl_6$ LHPs for different magnetic field strengths of 7.05, 14.1, 21.14, and 35.25 T (bottom to top) under non–spinning conditions using the NMR parameters listed in Table 2. Resolution between the high frequency horns of four–coordinate Cl ($^{[4]}Cl$) of $CsPb_2Cl_5$ and $Cs_4PbCl_6$ is lost from 14.1 T onwards.

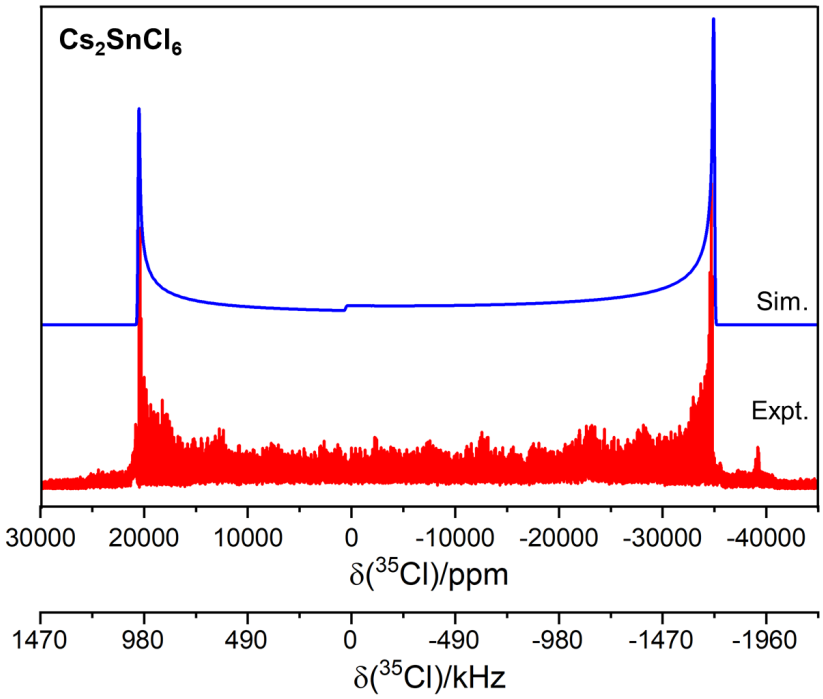


**Figure S8**. Non–spinning $^{35}Cl$ WURST–CPMG (red) and simulated (blue) spectra of $Cs_2SnCl_6$ acquired at 11.75 T. Reproduced from Karmakar, A.; Mukhopadhyay, S.; Gachod, P. G.; Mora–Gomez, V. A.; Bernard, G. M.; Brown, A. and Michaelis, V. K. *Chem. Mater.*, **2021**, *33*, 6078–6090, with permission from the American Chemical Society.

# Quantum Chemical Computational Data

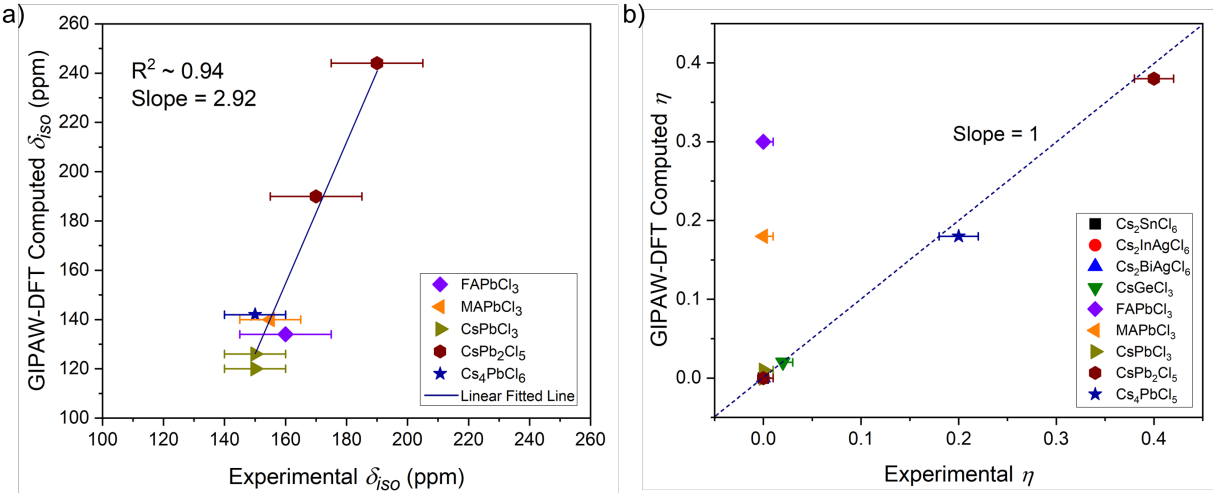


**Figure S9.** Comparison of the experimental with GIPAW–DFT computed $^{35}$Cl (a) $\delta_{iso}$ of LHPs and (b) $\eta$ of MHPs listed in Table 2. The computed $\eta$ values of FA– (violet ♦) and $MAPbCl_3$ (orange ◀) deviated from the expected trend displayed by the dotted line with slope = 1 due to $^{1}$H positions on the mobile A–site cations.

GIPAW–DFT computed $^{35}$Cl magnetic shielding tensor values of the secondary reference CsCl were $\sigma_{11} = \sigma_{22} = \sigma_{33} = 800.75$ ppm. Using the relation:

$$\delta(\text{ppm}) \approx (\sigma_{ref} - \sigma_{computed})\ \text{ppm} = (\sigma_{ref} - 800.75)\ \text{ppm},$$

and $\delta_{iso} = 114$ ppm found from the experimental $^{35}$Cl solid CsCl spectrum at 7.05 T as discussed before, the $\sigma_{ref}$ value was found to be 914.75 ppm (*i.e.*, $\sigma_{ref} = \delta + \sigma_{computed}$ in ppm).

This value of $\sigma_{ref}$ was used to obtain the calculated $\delta_{iso}$ values for all the samples using the following equations: $\delta_{ii}(\text{ppm}) = (914.75 - \sigma_{ii,computed})$ ppm, where $i = 1, 2, 3$, and $\delta_{iso} = (\delta_{11} + \delta_{22} + \delta_{33})/3$.

**Table S6.** GIPAW–DFT computed $^{35}$Cl NMR parameters for $Cs_2SnCl_6$, $Cs_2InAgCl_6$, $Cs_2BiAgCl_6$, $CsGeCl_3$ and $Cs_4PbCl_6$ with single Cl site.

| Materials | Magnetic Shielding Tensor (ppm) | | | $\delta_{iso}$ (ppm) | $C_Q$ (MHz) | $\eta$ | EFG Tensor | | | |
|---|---|---|---|---|---|---|---|---|---|---|
| | | | | | | | $V_{ZZ}$ (au) | Euler Angles (Degree) | | |
| | $\sigma_{11}$ | $\sigma_{22}$ | $\sigma_{33}$ | | | | | α | β | γ |
| $Cs_2SnCl_6$ | 251.67 | 251.67 | 900.95 | 447 | −33.54 | 0 | 1.75 | 0 | 0 | 0 |
| $Cs_2InAgCl_6$ | 708.78 | 708.78 | 921.59 | 135 | −29.02 | 0 | 1.51 | 0 | 0 | 0 |
| $Cs_2BiAgCl_6$ | 786.99 | 786.99 | 868.16 | 101 | −25.34 | 0 | 1.32 | 0 | 0 | 0 |
| $CsGeCl_3$ | 609.19 | 651.76 | 863.56 | 207 | −25.30 | 0.02 | 1.32 | 90 | 0.79 | 0 |
| $Cs_4PbCl_6$ | 725.01 | 771.33 | 821.90 | 142 | −8.92 | 0.18 | 0.47 | 65.10 | 11.64 | 69.98 |

**Table S7.** GIPAW–DFT computed $^{35}$Cl NMR parameters for $FAPbCl_3$.

| Cl Sites | Magnetic Shielding Tensor (ppm) | | | $\delta_{iso}$ (ppm) | $C_Q$ (MHz) | $\eta$ | EFG Tensor | | | |
|---|---|---|---|---|---|---|---|---|---|---|
| | | | | | | | $V_{ZZ}$ (au) | Euler Angles (Degree) | | |
| | $\sigma_{11}$ | $\sigma_{22}$ | $\sigma_{33}$ | | | | | α | β | γ |
| Cl(1) | 723.95 | 739.66 | 945.94 | 112 | –18.89 | 0.42 | 0.98 | 90 | 0 | 0 |
| Cl(2) | 640.17 | 670.70 | 909.10 | 175 | –21.29 | 0.35 | 1.11 | 90 | 0 | 0 |
| Cl(3) | 739.53 | 754.85 | 902.03 | 116 | –15.23 | 0.14 | 0.79 | 90 | 0 | 0 |

*Note.* Three different Cl atoms along the coordinate axes arises after the hydrogen insertion in the organic FA cation. Average values of $C_Q$, $\eta$ and $\delta_{iso}$ are listed in Table 2 for the single $^{35}$Cl site of $FAPbCl_3$.

**Table S8.** GIPAW–DFT computed $^{35}$Cl NMR parameters for $MAPbCl_3$.

| Cl Sites | Magnetic Shielding Tensor (ppm) | | | $\delta_{iso}$ (ppm) | $C_Q$ (MHz) | $\eta$ | EFG Tensor | | | |
|---|---|---|---|---|---|---|---|---|---|---|
| | | | | | | | $V_{ZZ}$ (au) | Euler Angles (Degree) | | |
| | $\sigma_{11}$ | $\sigma_{22}$ | $\sigma_{33}$ | | | | | α | β | γ |
| Cl(1) | 678.70 | 709.71 | 932.92 | 141 | –18.90 | 0.16 | 0.99 | 316.49 | 1.87 | 70.03 |
| Cl(2) | 690.37 | 721.03 | 944.47 | 129 | –18.61 | 0.09 | 0.97 | 141.69 | 1.80 | 298.63 |
| Cl(3) | 686.68 | 697.72 | 912.38 | 149 | –17.20 | 0.29 | 0.90 | 223.08 | 3.77 | 253.93 |

*Note.* Three different Cl atoms along the coordinate axes arises after the hydrogen insertion in the organic MA cation. Average values of $C_Q$, $\eta$ and $\delta_{iso}$ are listed in Table 2 for the single $^{35}$Cl site of $MAPbCl_3$.

**Table S9.** GIPAW–DFT computed $^{35}$Cl NMR parameters for $CsPbCl_3$.

| Cl Sites | Magnetic Shielding Tensor (ppm) | | | $\delta_{iso}$ (ppm) | $C_Q$ (MHz) | $\eta$ | EFG Tensor | | | |
|---|---|---|---|---|---|---|---|---|---|---|
| | | | | | | | $V_{ZZ}$ (au) | Euler Angles (Degree) | | |
| | $\sigma_{11}$ | $\sigma_{22}$ | $\sigma_{33}$ | | | | | α | β | γ |
| Cl(1) | 719.74 | 745.10 | 903.21 | 126 | –16.52 | 0.01 | 0.86 | 359.54 | 0.17 | 267.84 |
| Cl(2) | 730.59 | 736.12 | 918.42 | 120 | –16.92 | 0 | 0.88 | 95.19 | 0 | 0 |

**Table S10.** GIPAW–DFT computed $^{35}$Cl NMR parameters for $CsPb_2Cl_5$.

| Cl Sites | Magnetic Shielding Tensor (ppm) | | | $\delta_{iso}$ (ppm) | $C_Q$ (MHz) | $\eta$ | EFG Tensor | | | |
|---|---|---|---|---|---|---|---|---|---|---|
| | | | | | | | $V_{ZZ}$ (au) | Euler Angles (Degree) | | |
| | $\sigma_{11}$ | $\sigma_{22}$ | $\sigma_{33}$ | | | | | α | β | γ |
| Cl(1) | 743.66 | 741.47 | 688.22 | 190 | –8.59 | 0.38 | 0.45 | 0 | 18.85 | 0 |
| Cl(2) | 692.69 | 692.69 | 626.95 | 244 | 15.34 | 0 | 0.80 | 90 | 90 | 180 |

**Table S11.** Experimental and GIPAW–DFT computed fraction of $^{35}Cl$ sites in the samples with multiple Cl sites.

| Samples | CN | Local Cl Environment | % Fraction of $^{35}Cl$ Sites | |
|---|---|---|---|---|
| | | | Experimental | GIPAW–DFT |
| $CsPbCl_3$ | 2 | $Pb_2$ non–collinear (Pb–Cl–Pb bond angle ~161°) | 62 | 67 |
| | 2 | $Pb_2$ non–collinear (Pb–Cl–Pb bond angle ~169°) | 38 | 33 |
| $CsPb_2Cl_5$ | 3 | $Pb_3$ trigonal pyramidal | 80 | 80 |
| | 4 | $Pb_4$ square planar | 20 | 20 |

a) $Cs_2SnCl_6$

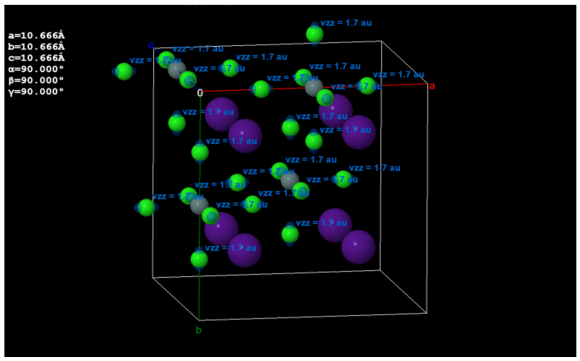


b) $Cs_2InAgCl_6$

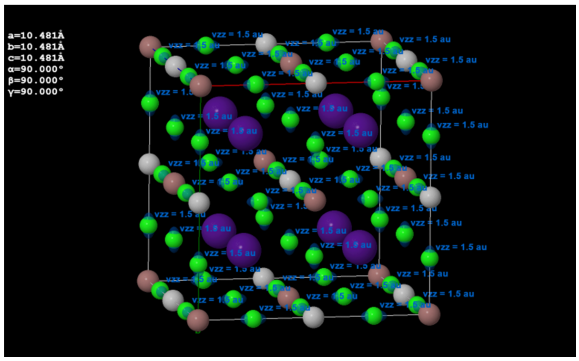


c) $Cs_2BiAgCl_6$

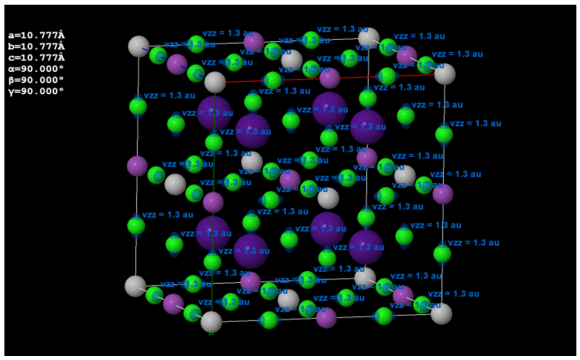


d) $CsGeCl_3$

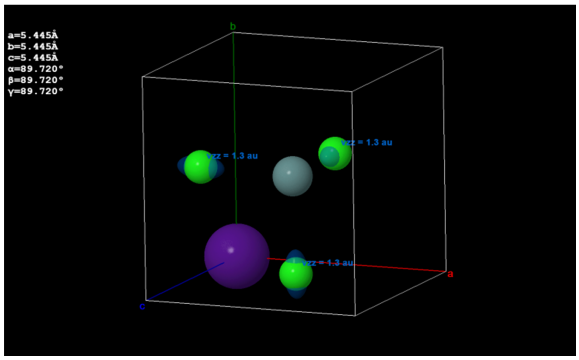


e) $FAPbCl_3$

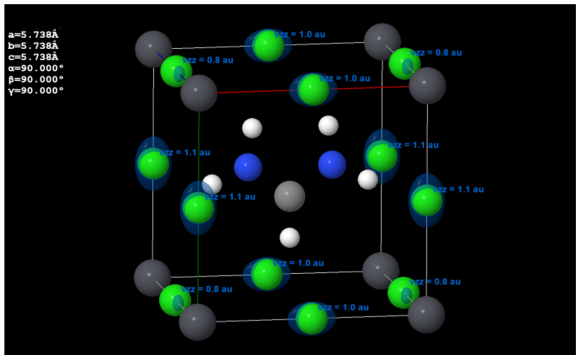


f) $MAPbCl_3$

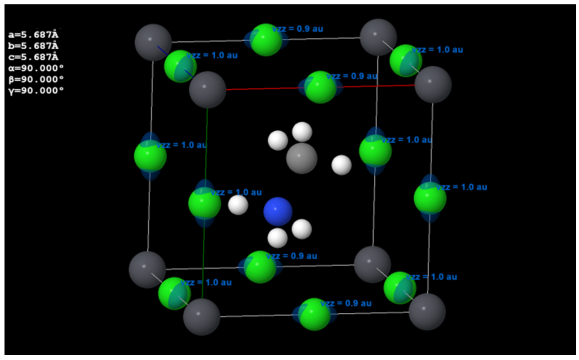

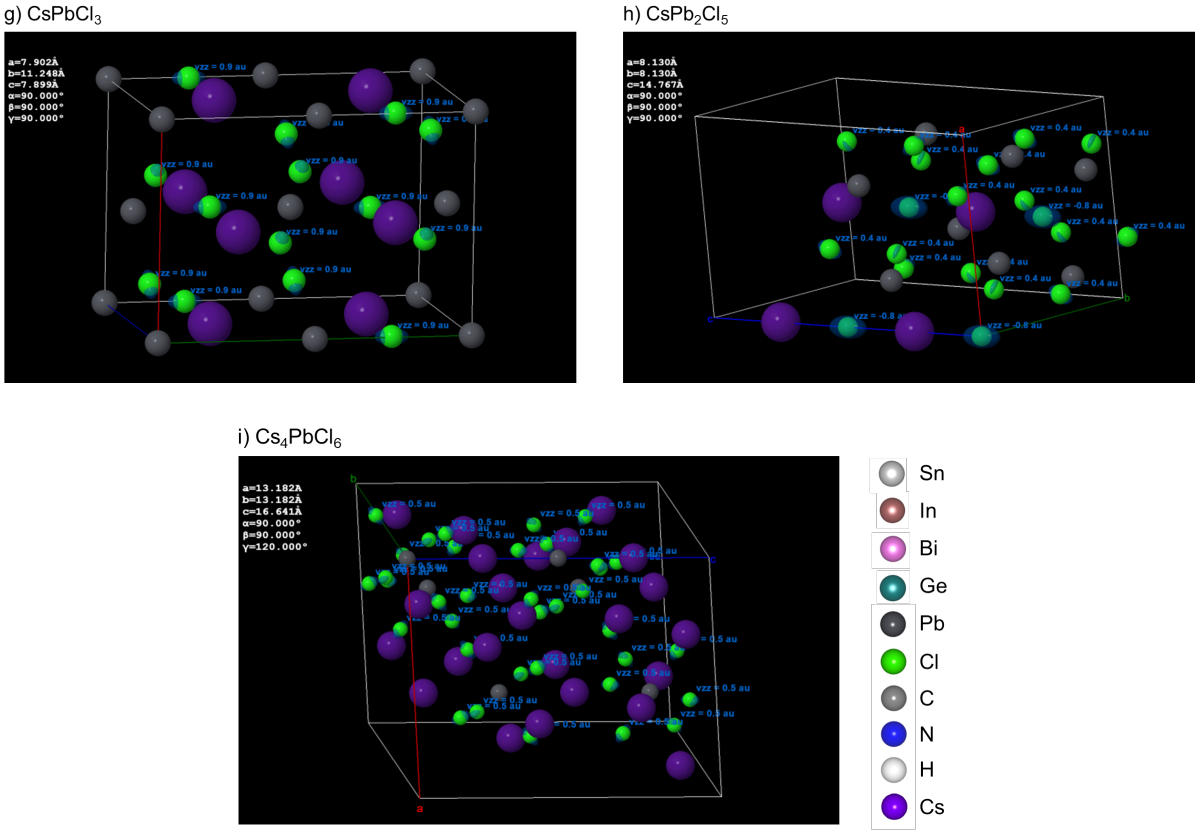


**Figure S10.** The computed EFG ellipsoids around the $^{35}$Cl atoms of (a) $Cs_2SnCl_6$, (b) $Cs_2InAgCl_6$, (c) $Cs_2BiAgCl_6$, (d) $CsGeCl_3$, (e) $FAPbCl_3$, (f) $MAPbCl_3$, (g) $CsPbCl_3$, (h) $CsPb_2Cl_5$, and (i) $Cs_4PbCl_6$. Of interest, $V_{ZZ}$ for all Cl atoms is aligned along its Pb–Cl bond except for four-coordinate Cl ($^{[4]}$Cl) in $CsPb_2Cl_5$ in (d).

# References


(1) Karmakar, A.; Dodd, M. S.; Zhang, X.; Oakley, M. S.; Klobukowski, M.; Michaelis, V. K. Mechanochemical Synthesis of 0D and 3D Cesium Lead Mixed Halide Perovskites. *Chem. Commun.* **2019**, *55*, 5079–5082.

(2) Karmakar, A.; Askar, A. M.; Bernard, G. M.; Terskikh, V. V.; Ha, M.; Patel, S.; Shankar, K.; Michaelis, V. K. Mechanochemical Synthesis of Methylammonium Lead Mixed–Halide Perovskites: Unraveling the Solid–Solution Behavior Using Solid–State NMR. *Chem. Mater.* **2018**, *30*, 2309–2321.

(3) Karmakar, A.; Bernard, G. M.; Meldrum, A.; Oliynyk, A. O.; Michaelis, V. K. Tailorable Indirect to Direct Band–Gap Double Perovskites with Bright White–Light Emission: Decoding Chemical Structure Using Solid–State NMR. *J. Am. Chem. Soc.* **2020**, *142*, 10780–10793.

(4) Hooper, R. W.; Ni, C.; Tkachuk, D. G.; He, Y.; Terskikh, V. V.; Veinot, J. G. C.; Michaelis, V. K. Exploring Structural Nuances in Germanium Halide Perovskites Using Solid–State $^{73}$Ge and $^{133}$Cs NMR Spectroscopy. *J. Phys. Chem. Lett.* **2022**, *13*, 1687–1696.

(5) Rodriguez–Carvajal, J. FULLPROF: A Program for Rietveld Refinement and Pattern Matching Analysis. In *Abstracts of the Satellite Meeting on Powder Diffraction of the XV Congress of the IUCr*; Toulouse, France, **1990**; p 127.

(6) O'Dell, L. A.; Schurko, R. W. QCPMG Using Adiabatic Pulses for Faster Acquisition of Ultra–Wideline NMR Spectra. *Chem. Phys. Lett.* **2008**, *464*, 97–102.

(7) O'Dell, L. A. The WURST Kind of Pulses in Solid–State NMR. *Solid State Nucl. Magn. Reson.* **2013**, *55–56*, 28–41.

(8) Massiot, D.; Farnan, I.; Gautier, N.; Trumeau, D.; Trokiner, A.; Coutures, J. P. $^{71}$Ga and $^{69}$Ga Nuclear Magnetic Resonance Study of β−$Ga_2O_3$: Resolution of Four− and Six−Fold Coordinated Ga Sites in Static Conditions. *Solid State Nucl. Magn. Reson.* **1995**, *4*, 241–248.
(9) Hahn, E. L. Spin Echoes. *Phys. Rev.* **1950**, *80*, 580.
(10) Weisman, I. D.; Bennett, L. H. Quadrupolar Echoes in Solids. *Phys. Rev.* **1969**, *181*, 1341.
(11) Davis, J. H.; Jeffrey, K. R.; Bloom, M.; Valic, M. I.; Higgs, T. P. Quadrupolar Echo Deuteron Magnetic Resonance Spectroscopy in Ordered Hydrocarbon Chains. *Chem. Phys. Lett.* **1976**, *42*, 390–394.
(12) Klaus Eichele. Wsolids1 NMR Simulation Package, 1.21.7., Universität Tübingen http://anorganik.uni−tuebingen.de/klaus/soft/index.php?p=wsolids1/wsolids1 (accessed Sep 28, 2021).
(13) Adiga, S.; Aebi, D.; Bryce, D. L. EFGShield — A Program for Parsing and Summarizing the Results of Electric Field Gradient and Nuclear Magnetic Shielding Tensor Calculations. *Can. J. Chem.* **2011**, *85*, 496–505.
(14) Sturniolo, S.; Green, T. F. G.; Hanson, R. M.; Zilka, M.; Refson, K.; Hodgkinson, P.; Brown, S. P.; Yates, J. R. Visualization and Processing of Computed Solid−State NMR Parameters: MagresView and MagresPython. *Solid State Nucl. Magn. Reson.* **2016**, *78*, 64–70.
(15) Clark, S. J.; Segall, M. D.; Pickard, C. J.; Hasnip, P. J.; Probert, M. I. J.; Refson, K.; Payne, M. C. First Principles Methods Using CASTEP. *Zeitschrift für Krist. − Cryst. Mater.* **2005**, *220*, 567–570.
(16) Segall, M. D.; Lindan, P. J. D.; Probert, M. J.; Pickard, C. J.; Hasnip, P. J.; Clark, S. J.; Payne, M. C. First−Principles Simulation: Ideas, Illustrations and the CASTEP Code. *J. Phys. Condens. Matter* **2002**, *14*, 2717.
(17) Pickard, C. J.; Mauri, F. All−Electron Magnetic Response with Pseudopotentials: NMR Chemical Shifts. *Phys. Rev. B* **2001**, *63*, 245101.
(18) Yates, J. R.; Pickard, C. J.; Mauri, F. Calculation of NMR Chemical Shifts for Extended Systems Using Ultrasoft Pseudopotentials. *Phys. Rev. B* **2007**, *76*, 024401.
(19) Perdew, J. P.; Burke, K.; Ernzerhof, M. Generalized Gradient Approximation Made Simple. *Phys. Rev. Lett.* **1996**, *77* (18), 3865.
(20) Monkhorst, H. J.; Pack, J. D. Special Points for Brillouin−Zone Integrations. *Phys. Rev. B* **1976**, *13*, 5188.
(21) Hanwell, M. D.; Curtis, D. E.; Lonie, D. C.; Vandermeersch, T.; Zurek, E.; Hutchison, G. R. Avogadro: An Advanced Semantic Chemical Editor, Visualization, and Analysis Platform. *J. Cheminformatics* **2012**, *4*, 1–17.
(22) Avogadro: an open−source molecular builder and visualization tool. Version 1.2.0n−win32 http://avogadro.cc/ (accessed Sep 1, 2021).
(23) Persson, K. Materials Data on $Cs_2SnCl_6$ (SG:225) by Materials Project https://materialsproject.org/materials/mp−608555/ (accessed Aug 30, 2021).
(24) Zhou, J.; Xia, Z.; Molokeev, M. S.; Zhang, X.; Peng, D.; Liu, Q. Composition Design, Optical Gap and Stability Investigations of Lead−Free Halide Double Perovskite $Cs_2AgInCl_6$. *J. Mater. Chem. A* **2017**, *5*, 15031–15037.
(25) McClure, E. T.; Ball, M. R.; Windl, W.; Woodward, P. M. $Cs_2AgBiX_6$ (X = Br, Cl): New Visible Light Absorbing, Lead−Free Halide Perovskite Semiconductors. *Chem. Mater.* **2016**, *28*, 1348–1354.
(26) Thiele, G.; Rotter, H. W.; Schmidt, K. D. Kristallstrukturen Und Phasentransformationen von Caesiumtrihalogenogermanaten(II) $CsGeX_3$ (X = Cl, Br, I). *Zeitschrift für Anorg. und Allg. Chemie* **1987**, *545*, 148–156.
(27) Govinda, S.; Kore, B. P.; Swain, D.; Hossain, A.; De, C.; Row, T. N. G.; Sarma, D. D. Critical Comparison of $FAPbX_3$ and $MAPbX_3$ (X = Br and Cl): How Do They Differ? *J. Phys. Chem. C* **2018**, *122*, 13758–13766.
(28) Chen, K.; Deng, X.; Goddard, R.; Tüysüz, H. Pseudomorphic Transformation of Organometal Halide Perovskite Using the Gaseous Hydrogen Halide Reaction. *Chem. Mater.* **2016**, *28*, 5530–5537.
(29) Linaburg, M. R.; McClure, E. T.; Majher, J. D.; Woodward, P. M. $Cs_{1-x}Rb_xPbCl_3$ and $Cs_{1-}$

$_x$Rb$_x$PbBr$_3$ Solid Solutions: Understanding Octahedral Tilting in Lead Halide Perovskites. *Chem. Mater.* **2017**, *29*, 3507–3514.
(30) Chen, Y.; Molokeev, M. S.; Atuchin, V. V; Reshak, A. H.; Auluck, S.; Alahmed, Z. A.; Xia, Z. Synthesis, Crystal Structure, and Optical Gap of Two−Dimensional Halide Solid Solutions $CsPb_2(Cl_{1-x}Br_x)_5$. *Inorg. Chem.* **2018**, *57*, 9.
(31) Cenzual, K.; Gelato, L. M.; Penzo, M.; Parthé, E. Overlooked Trigonal Symmetry in Structures Reported with Monoclinic Centred Bravais Lattices; Trigonal Description of $Li_8Pb_3$, PtTe, $Pt_3Te_4$, $Pt_2Te_3$, $LiFe_6Ge_4$, $LiFe_6Ge_5$, $CaGa_6Te_{10}$ and $La_{3.266}Mn_{1.1}S_6$. *Zeitschrift für Krist. – Cryst. Mater.* **1990**, *193*, 217–242.
(32) Cortona, P. Direct Determination of Self−Consistent Total Energies and Charge Densities of Solids: A Study of the Cohesive Properties of the Alkali Halides. *Phys. Rev. B* **1992**, *46*, 2008.
(33) Duer, M. J. *Solid−State NMR Spectroscopy: Principles and Applications*; Duer, M. J., Ed.; Blackwell Science Ltd., **2002**.
(34) Bryce, D. L.; Wasylishen, R. E. Quadrupolar Nuclei in Solids: Influence of Different Interactions on Spectra. *Encycl. Magn. Reson.* **2011**.